PERGAMON

Journal of Structural Geology 25 (2003) 1301–1316

JOURNAL OF STRUCTURAL GEOLOGY

www.elsevier.com/locate/jsg

The fractal geometry of some stylolites from the Calcare Massiccio Formation, Italy

Zvi Karcz*, Christopher H. Scholz

Lamont-Doherty Earth Observatory and Department of Earth and Environmental Sciences, Columbia University, P.O. Box 1000, 61 Route 9W, Palisades, New York, USA

Received 22 May 2001; accepted 7 September 2002

Abstract

Stylolites are serrated surfaces that form by stress enhanced dissolution. Though their geometry and morphology reflects their formation and evolution, only a few studies have attempted to quantify them. Here we present results indicating that stylolites in limestone of the Calcare Massiccio Formation (Jurassic, Italy) are fractal over 4.5 orders of magnitude in spatial bandwidth, with an average fractal dimension (obtained by spectral and scaled windowed variance analyses) clustering at 1.47. Some stylolites from the Skene (Cambrian, USA) and Tamar (Cenomanian, Israel) formations are fractal over 3 orders of magnitude, with fractal dimensions of 1.26 and 1.43. These values are high relative to other natural surfaces, and reflect the jagged topography of the stylolites. Preliminary results indicate that the fractal dimension and power are constant throughout the stylolite surface, and are not orientation dependent. Furthermore, we show that stylolite contours are fractal too. The grain size does not register in our analyses, implying that the grain is not a cutoff between processes. Rather, stylolite generating processes operate similarly below and above the grain size. Our results suggest that the geometry of these stylolites, especially at long wavelengths, may not be sensitive to the immediate fabric surrounding them.

Keywords: Stylolites; Fractals; Mass transfer creep; Pressure solution; Dissolution cleavage; Anticrack

1. Introduction

Mass transfer creep (MTC), commonly termed pressure solution creep, is a major rock deformation process that involves material dissolution, diffusion and precipitation at low PT conditions (Paterson, 1973; Rutter, 1983). Its impact on rocks is both extensive and varied. Primarily, it accounts for significant amounts of strain in certain rocks (e.g. Alvarez et al., 1978), but it also modifies porosity and permeability (Ortoleva et al., 1995; Langer et al., 1999) which may alter the strength of faults (Sleep and Blanpied, 1992). Furthermore, rates of MTC were shown to control the slip behavior of gauge bearing faults (Bos et al., 2000; Kanagawa et al., 2000). Finally, strain due to pressure solution is thought to cause discrepancies in strain rates measured along active faults (e.g. North, 1974; Dolan et al., 1995; Duebendorfer et al., 1998), and therefore is an important component of seismic hazard analysis.

Pressure solution deformation is traditionally classified as pervasive or localized (Tada and Siever, 1989). The former, commonly termed intergranular pressure solution (IPS) occurs at grain contacts; the latter operates along discrete surfaces of dissolution. These two modes of pressure solution are not mutually exclusive and often occur in the same rock body. The difference between them is not only morphological, but probably reflects a more fundamental difference in the governing processes on the atomic scale or in the rates of the various sub-processes at the grain contact (e.g. Dewers and Ortoleva, 1990).

The present study focuses on geometrical aspects of a unique type of localized pressure solution known as 'stylolites'. Stylolites are serrated surfaces of dissolution lined with insoluble material (e.g. Bathurst, 1995). Stockdale (1922, 1926) suggested that these surfaces form in lithified sediments and terminate laterally, and that the detritus and clay within them are a residue of the dissolved rock. Stylolites were later shown to form in various lithologies (Park and Schot, 1968) and to exhibit a wide range of geometry and field relations. They are broadly classified by their geometry (e.g. Park and Schot, 1968;

* Corresponding author.

0191-8141/03/$ - see front matter © 2003 Elsevier Science Ltd. All rights reserved.
PII: S0191-8141(02)00173-6

Wanless, 1979; Guzzetta, 1984) and orientation with respect to bedding (Park and Schot, 1968).

Despite the impressive volume of work spanning numerous lithologies and geological settings, fundamental issues concerning the structure and formation of stylolites are still unresolved. One such issue is the geometry of stylolites and its relationship to the fabric and composition of the host rock. Progress here was inhibited mainly because most studies are descriptive and qualitative, rather than quantitative. A quantitative characterization of the geometry of stylolites will facilitate comparison between similar stylolites and different segments of the same stylolite, and will offer a powerful tool in assessing models of stylolite formation.

In the last two decades the geometry of natural surfaces, from molecules and proteins to ocean floors and planet relief has been studied extensively by fractal analysis. Stylolites, especially the seismogram type (sensu Park and Schot, 1968), lend themselves to such analysis since their profiles 'seem fractal'—they look the same on many scales of observation. This scale invariance is the basic feature of fractal objects, and is commonly observed in natural surfaces only in a restricted waveband (Voss, 1988.) The lower and upper limits of this fractal band are the first important geometrical parameter of an object, often reflecting a characteristic length scale, with some physical significance. For example, in faults the lower and upper fractal limits correspond to the grain size of the rock and the thickness of the seismogenic crust, respectively (Scholz, 1995). The two other fundamental fractal parameters characterize the jaggedness of the object (i.e. the fractal dimension) and its steepness (e.g. the crossover length, discussed below).

Geometrical scale invariance within the fractal band suggests formation by processes that act similarly throughout the band, with no characteristic wavelength (e.g. Turcotte, 1992). For the study of stylolites, which have never been produced experimentally due to their slow rates of formation (Tada and Siever, 1989), this is particularly important. If stylolites are shown to be scale invariant down to wavelengths shorter than the grain size, the experimentally observed processes and structures at sub-millimeter grain contacts (e.g. Hickman and Evans, 1995; Den Brok, 1998) may be relevant to those of stylolites. At the very least, a quantitative statement can be made on the link between macroscopic and microscopic features and processes of pressure solution.

Finally, clays in carbonate and siliceous rocks are known to affect the nucleation and evolution of stylolites. Observations suggest that the higher the clay content in the rock the smoother the stylolite (e.g. Barrett, 1964). Furthermore, clay is known to significantly enhance processes of pressure solution (e.g. Heald, 1955; Hickman and Evans, 1995). Early studies indicate that clays lining stylolites are similar to those in the ambient rock, but subsequent studies show a distinct variation suggesting growth of authigenic minerals on the stylolite surface (e.g. Lind and Schioler, 1994). If indeed stylolites are sites of mineral alteration, nucleation and growth, one may assume that these processes have some effect on the geometry of the stylolite, and its evolution. In this study we compare the clay composition in the stylolites and the ambient rock to address this issue.

We show here that the studied stylolites are fractal surfaces with no apparent limits to their fractal band. The clays in the stylolites are the same as in the host rocks, suggesting that the stylolites were not a unique site of authigenesis.

2. Data collection

Our study focused on stylolites in limestone from the Calcare Massiccio (CM) Formation (Lower Jurassic) of the Umbria–Marche of Central Italy. A 3-m-long, 1.2-m-wide and 2-cm-thick slab of this rock, known as 'American Pink Marble' in the decorative stone industry, was purchased at a local stone yard. This so-called 'marble' is a wackestone–packstone limestone, composed mainly of pellets and various bioclasts (planktic and benthic foramenifera and few fragments of pelecypod and gastropod shells). Variations in color, grain size and distribution, grain to matrix and cement ratio and stylolite type yield a straightforward division of the slab into four lithostratigraphic units. These units are bounded by stylolites CMa, CMc and CMe (Fig. 1).

Five of the most prominent stylolites in the slab were singled out for this study due to their continuity and apparent geometrical dissimilarity (Fig. 2). The stylolites are not contained within the slab, so their true length is unknown. The stylolites were digitized parallel to the slab face at two different scales (Table 1): a $\sim$2 m segment (macro-trace) of each stylolite was digitized at 0.5 mm increments, and a $\sim$4 cm segment (micro-trace) of each stylolite was digitized at 25 μm increments. Both large- and small-scale digitizations were done with a Lasico1282W-24 digitizer, the first directly on the slab and the latter on enlarged images ($\times$16) of thin sections of the stylolites. The largest wavelength recorded is the length of the measured profile (255 and 4.35 cm, respectively), and the smallest wavelength recorded is twice the sampling interval (the Nyquist wavelength, 1 and 0.05 mm, respectively). Thus, the combined measurements span over four orders of magnitude, with large- and small-scale measurements overlapping in the 1 mm to 4.35 cm waveband.

Stylolites from three other lithologies were studied for comparison (Fig. 3): a Cenomanian biomicritic limestone of the Hatzera Formation from the Negev, Israel; a Cambrian siliciclastic limestone of the Skene Formation from New York State, USA; and a micritic limestone from China known in the decorative stone industry as 'Mystique Dark' (age and provenance unknown). These were only studied at a small scale: their traces were digitized from enlarged

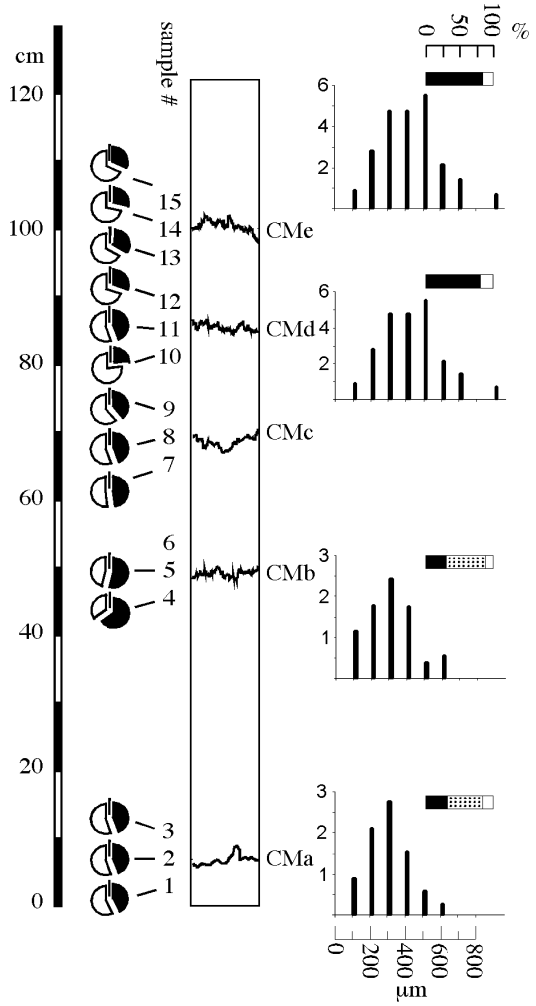

Fig. 1. Columnar section of the Calcare Massiccio slab. Lithological units are bounded by stylolites CMa, CMc and CMe. Grain size distribution (area covered by given grain size, in mm^2), and grain–matrix–cement ratio (horizontal bars on the right—black is grains, stippled is matrix, white is cement) estimates are based on point counting of >300 grains per diagram. Pie diagrams display clay composition of the samples—black is illite and white is kaolinite. Fe–chlorite concentrations are too small to be resolved on these diagrams (see Table 4).

images (×36) of thin sections with a sampling step of ~11 microns with a Didger digitizer.

Since the data processing of the profiles demands that the analyzed traces be monotonic, overhangs were removed during digitization. Overhangs are not abundant in the digitized traces and are deflected less than 10° from the vertical, and thus we assume that their removal does not modify significantly the values of the fractal dimension obtained. Furthermore, we point out that when digitizing a long profile of a seismogram-type stylolite, it is impossible to completely avoid overhangs no matter the inclination of the profile with respect to the stylolite plane, since they are wavy in all directions and on many scales.

Stylolites were studied here both in profile, where the plane of observation is normal to the plane of the stylolite (Figs. 2 and 3), and in contour, where the plane of observation is parallel to the plane of the stylolite (Fig. 4).

Sampling and preparation of samples for chemical analysis were conducted as follows: 10 ~40 g samples of ambient rock, and five ~25 g samples of stylolite rock were crushed, carbonate was dissolved with diluted hydrochloric acid (~1%) then dried and weighed (see Fig. 1 for sample location). Iron oxides, amorphous silica and alumina were extracted from the <75 μm fraction by standard procedures (Biscaye, 1965). The samples were then divided by sieving and settling to <2 μm, 2–20 μm and >20 μm fractions. The two smaller fractions were analyzed by XRD. Four samples were further glycolated to separate the smectite and chlorite peaks at $2\theta \sim 6°$, and subsequently analyzed. In addition, three samples of the >75 μm fraction were analyzed to determine the composition of the non-clay residue. Only CM samples were subjected to clay analysis.

3. Data analysis

The fractal dimension D is defined by considering a line of length L and a ruler of length d, so that:

$$L(d) = Ad^{1-D} \tag{1}$$

where A is a prefactor.

The fractal dimension is bounded from below by the topological dimension and from above by the Euclidean dimension. For example, a line has a topological dimension of one and a Euclidean dimension of two and thus $1 < D < 2$. Within these limits, the higher the fractal dimension, the more jagged the line.

One of the important characteristics of a fractal is that the "…shape is made of parts similar to the whole in some way" (Mandelbrot, in Feder, 1988). Objects that obey (1) are termed self-similar, indicating that they scale similarly in all directions. Strictly speaking, if $f(x,y)$ is statistically the same as $f(rx,ry)$, where r is a constant, the fractal is self-similar. However, if $f(x,y)$ is statistically similar to $f(rx, r^{Ha}y)$ ($0 < H_a < 1$, H_a is termed the Hausdorff measure) the fractal is defined as self-affine (Turcotte, 1992). Simply put, an image of a self-similar object (e.g. a map view of a coastline) needs to be magnified by the same value in both x and y directions to obtain a similar image. An image of a self-affine object on the other hand (e.g. a profile of topography) needs to be magnified more in the x direction than in the y direction to obtain a similar image. The distinction between self-similar and self-affine fractals is important, and the methods for analyzing them are different (e.g. Malinverno, 1990). Stylolites are viewed here both as profiles, in which case they are assumed to be self-affine, and as contours, in which case they are assumed to be self-similar.

The fractal dimension of a self-affine trace can be determined by various methods, all attempting to scale the

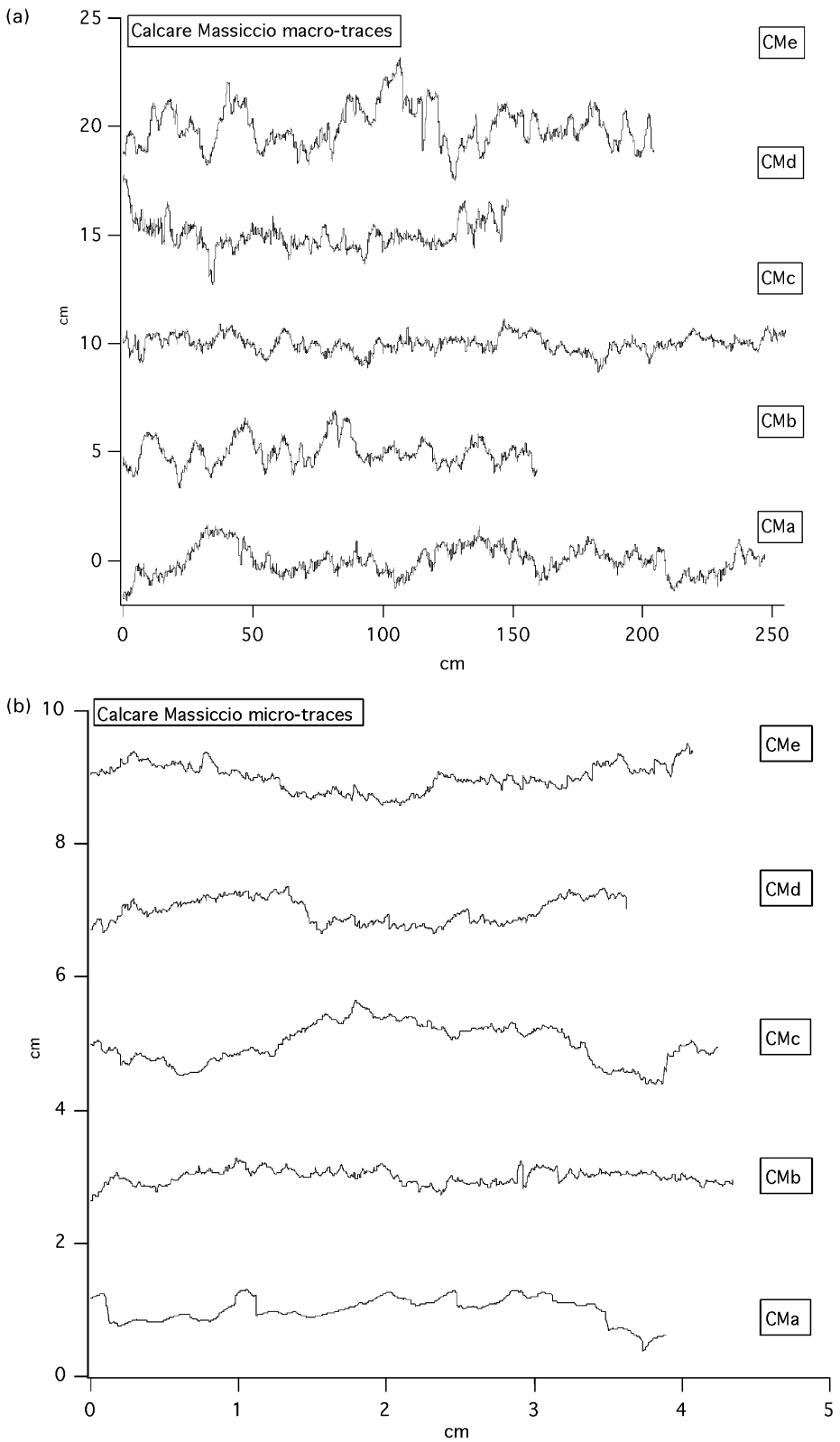

Fig. 2. Digitized traces of stylolite profiles in Calcare Massiccio slab. (a) Macro-traces with sampling interval of 0.5 mm (vertical exaggeration 10.5) and (b) micro-traces with sampling interval of 25 μm (vertical exaggeration of 0.7).

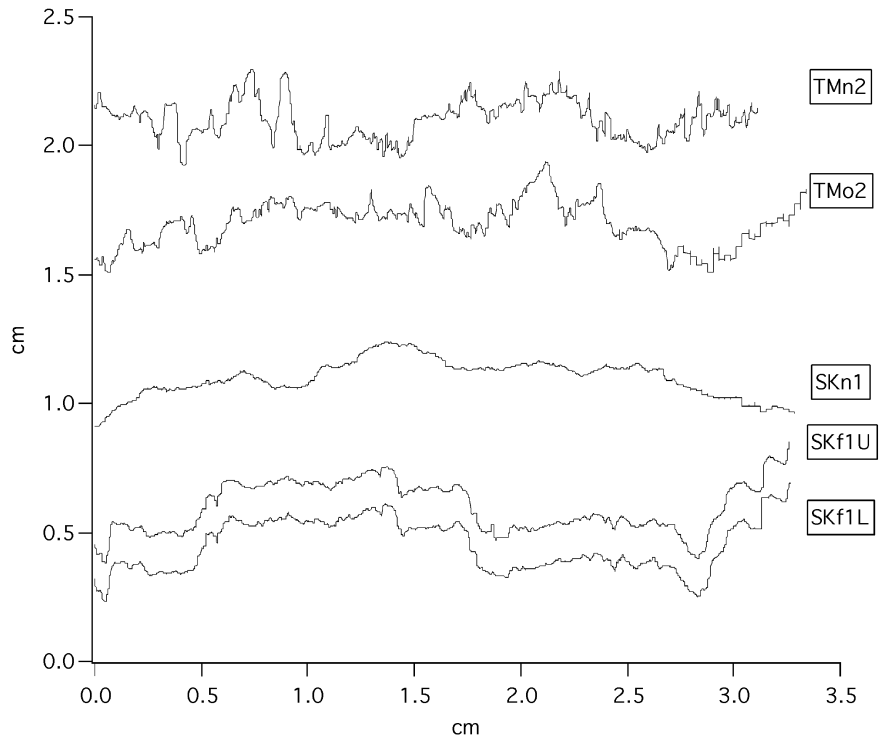

Fig. 3. Digitized traces of stylolite profiles in the Tamar Formation (TM) and the Skene Formation (SK), with sampling interval of 11 μm (vertical exaggeration of 2.7).

vertical axis with the horizontal one through a power law (e.g. Malamud and Turcotte, 1999). In the last 15 years considerable effort was directed, particularly in studies of human physiology, at assessing the robustness of these methods. We recommend the recent paper by Eke et al. (2002) and references within for in depth discussion and literature review. We follow here the procedure described in Cannon et al. (1997) for determining the fractal properties of

Table 1
Length and orientation of the traces analyzed in this study. Traces oriented normal to the plane of the stylolite are termed profiles, whereas those that are oriented parallel to the plane of the stylolite are termed contours

Trace	Lithology	Orientation wrt stylolite plane	Length[a] (points/cm)	Sampling interval (microns)
Micro-CMa	Calcare Massiccio	Normal	1557/3.89	25
Micro-CMb	Calcare Massiccio	Normal	1739/4.35	25
Micro-CMc	Calcare Massiccio	Normal	1696/4.24	25
Micro-CMd	Calcare Massiccio	Normal	1452/3.63	25
Micro-CMe	Calcare Massiccio	Normal	1630/4.08	25
Micro-CMbob1	Calcare Massiccio	Normal	630/1.58	25
Micro-CMbob2	Calcare Massiccio	Normal	666/1.67	25
Macro-CMa	Calcare Massiccio	Normal	4941/247.05	500
Macro-CMb	Calcare Massiccio	Normal	3182/159.1	500
Macro-CMc	Calcare Massiccio	Normal	5098.254.9	500
Macro-CMd	Calcare Massiccio	Normal	2966/148.3	500
Macro-CMe	Calcare Massiccio	Normal	4090/204.5	500
CMdp2	Calcare Massiccio	Parallel	9820/13.99	14
CMcp1	Calcare Massiccio	Parallel	21656/18.99	9
TMn2	Tamar Formation	Normal	2842/3.13	11
TMo2	Tamar Formation	Normal	3053/3.36	11
SKf1l	Skene Formation	Normal	2982/3.28	11
SKf1u	Skene Formation	Normal	2975/3.27	11
SKn1	Skene Formation	Normal	3001/3.3	11
SKp2	Skene Formation	Parallel	8031/9.46	12
MDa1	Mystique Dark tile	Parallel	8650/10.19	12

[a] Length for profiles is along *x*-axis; for contours is actual length.

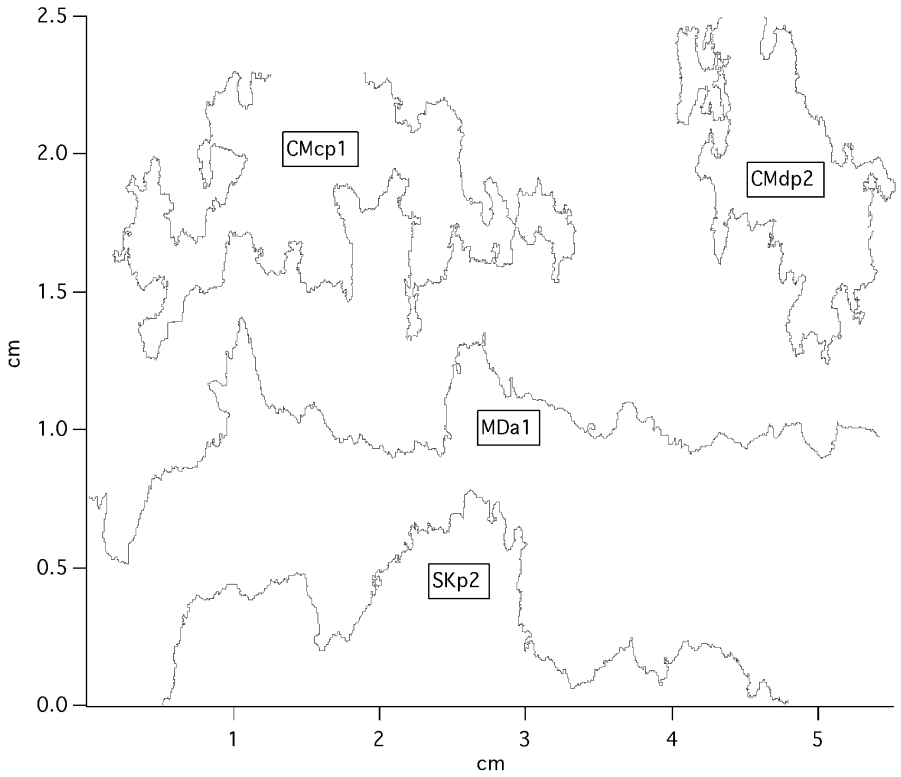

Fig. 4. Digitized traces of stylolite contours from the Calcare Massiccio slab (CM), the Skene Formation (SK), and the Mystique Dark tile (MD) with sampling intervals ranging from 9 to 14 μm (see Table 1) (vertical exaggeration of 1.9).

a 'real time series' (their section 5.2). First, the stationarity of the trace (i.e. whether the mean and variance of the trace change along the trace or as a function of its length) is established by spectral analysis. Spectral analysis quantifies the frequency content of a trace by transforming it from the physical domain to the frequency domain by the Fourier transform. The power spectral density (proportional to the amplitude squared) is then plotted against the frequency in log–log space. The highest and lowest frequencies are discarded to avoid aliasing and undersampling effects, respectively. Since measurements are not evenly distributed along the spectrum, data is binned, and finally a regression line is fitted. For a stationary trace the negative of the slope of the regression line (β) lies between -1 and 1, a range termed fractional Brownian noise, and for a non-stationary trace β lies between 1 and 3, a range termed fractional Brownian motion. The fractional Brownian motion range is further divided into persistent ($2 < \beta < 3$) and antipersistent ($1 < \beta < 2$). Persistence, often referred to as 'memory', indicates how correlated the trace is: in a persistent (antipersistent) trace, an increase is expected to be followed by an increase (decrease) (Feder, 1988). Spectral analysis also gives a first estimate of the fractal dimension, since the slope relates to the fractal dimension D_S by $\beta = 5 - 2D_S$ (Turcotte, 1992). In addition, breaks in the slope of the spectra or 'spikes' indicate cut-off frequencies or periodicities in the trace (e.g. Pelletier and Turcotte, 1999). Finally, the intercept with the log power axis (the power at frequency 1) is obtained to quantify the steepness of the trace.

If the traces are shown to be fractional Brownian motion, a battery of numerical tests termed 'scaled windowed variance' (SWV) methods are applied. These methods, described and examined thoroughly in Cannon et al. (1997), measure the variability of the trace at different scales as follows. The trace is divided into equal sized segments (commonly termed windows or lags); the mean in each segment is obtained and the standard deviation of the means plotted in log–log space of standard deviation versus window size; the procedure is repeated for windows of different sizes. The slope of the regression line through all points is termed the Hurst exponent H, and relates to the fractal dimension D_{SWV} by $D_{SWV} = 2 - H$. The three methods used here are termed standard (STD), bridge (BD) and linear regression (LD): the first uses the raw data in each segment, whereas the two others detrend each segment by removing the line connecting the first and last point (BD) or the regression line (LD) within the window. When fitting the regression line, the smallest windows (containing < 10 data points) and the largest windows (containing more than one-third of the data points) are excluded. At least 2^{15} data points are needed to distinguish at the 2% confidence level between two series with fractal dimensions differing by 0.1 (Cannon et al., 1997).

The crossover length reflects the steepness of the trace and may be simply defined as the length where the vertical

measure within the window (e.g. RMS roughness) equals the horizontal span of the window (w), or RMS(w) = w (e.g. Malinverno, 1991). We follow here this definition, though strictly speaking the SWV methods do not measure the roughness within each segment but the variability of the roughnesses between windows.

The standard windowed variance methods are closely related to the well-known and widely used rescaled range (or R/S) method introduced by Hurst (1951). The R/S method ties the range (R) of the trace, a measure of its greatest amplitude, to its length (τ) through a power law of the form:

$$\frac{R}{S} = \left(\frac{\tau}{2}\right)^{H} \tag{2}$$

where S is the standard deviation, and H ranges between 0.6 and 0.8 (Hurst et al., 1965). However, Bassingthwaighte and Raymond (1994, 1995) and others have shown that R/S analysis is unreliable for estimating the Hurst coefficient, especially for short traces ($<2^9$ data points). Thus, this classical method is avoided here.

The reason for using more than one method in determining the fractal dimension is that each method is sensitive to different properties of the trace. For example, since spectral analysis translates the complete trace into frequencies and amplitudes, it is not sensitive to local trends and variability; furthermore, it can present all values of β, whether positive or negative. It is, however, sensitive to edge effects and spectral leakage (Wilson, 2000). The SWV methods on the other hand are sensitive to local trends and variability, but saturate at $\beta > 3$ and $\beta < 1$. These differences suggest that one should not expect to obtain identical fractal dimension values from different methods (e.g. Malamud and Turcotte, 1999).

Preprocessing steps and their effects on a sample profile are presented in Fig. 5. A trace typically consists of a stochastic component, periodic components and a trend (Fig. 5a). In the case of parallel sub-horizontal stylolites studied here, the latter is an artifact and therefore is removed. Data points were then forced to be equally spaced (Fig. 5b), and finally tapered (Fig. 5c). Tapering is a standard procedure employed in spectral analysis to reduce spectral leakage, by forcing both ends of the trace to zero (e.g. Press et al., 1994). Though the tapered profile looks different than the original one, statistically the frequency and amplitude information is unharmed. Note that the traces were not tapered when analyzed by the windowed methods.

Stylolite contours, assumed to be self-similar, were analyzed by the ruler method, formally described in Eq. (1). The length of the trace $L(d)$ is measured with rulers of various sizes (d), to obtain a straight line in log trace log ruler space. The procedure used here (based on Middleton, 1999) measures the length of the trace with a given ruler size 10 times, starting the measurements at different points.

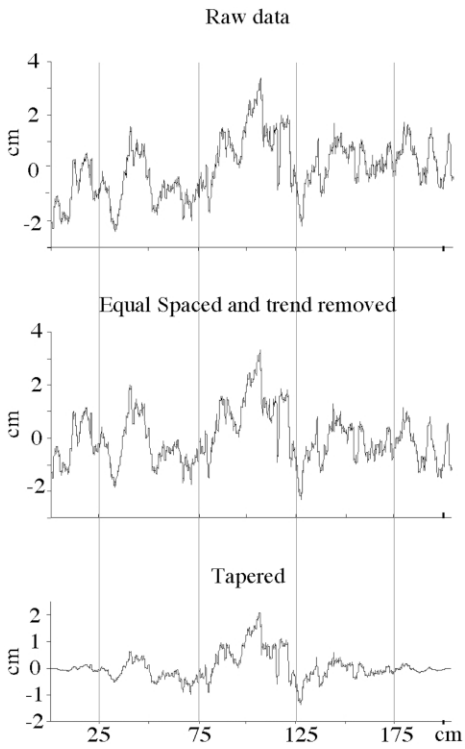

Fig. 5. Data processing illustrated on micro-trace of stylolite CMe. From top to bottom, raw data, equally spaced and detrended, and tapered. Note scale changes in vertical axis.

4. Measurements and results

The spectra of the Calcare Massiccio stylolite profiles are presented in Fig. 6, and fractal dimension and power values in Table 2. The slopes of the spectra lie between 1.84 and 2.34, with an average of 2.06. These values are within the fractional Brownian motion range, indicating that these stylolites are fractal over the measured bandwidth. Close inspection of the individual spectra reveals no significant spikes in any of them, though breaks in slopes are evident in micro-traces CMa, CMb and CMc (at a waveband of 1 to 3 mm) and macro-trace CMd (at a wavelength of 10 cm). The spectra of the micro- and macro-traces coincide in the overlapping waveband (1–40 mm), though gradual changes in slopes are evident—spectra of micro-traces CMa, CMc and CMd are steeper than their macro-trace counterparts, whereas that of micro-trace CMb is less steep than its macro-trace counterpart. Spectra of stylolites from the Tamar and Skene Formations are presented for comparison in Fig. 7. In both lithologies, no spikes are observed, though a slight change in slope is seen for trace SKn1, at a wavelength of 1 mm.

Since we are interested in the effects of grain size on the geometry of the stylolite, an additional spectral test was performed. Each micro-trace of the Calcare Massiccio slab was split into three equal segments of roughly 500 points, the spectra of each segment was obtained and the three spectra were averaged. This procedure significantly reduces

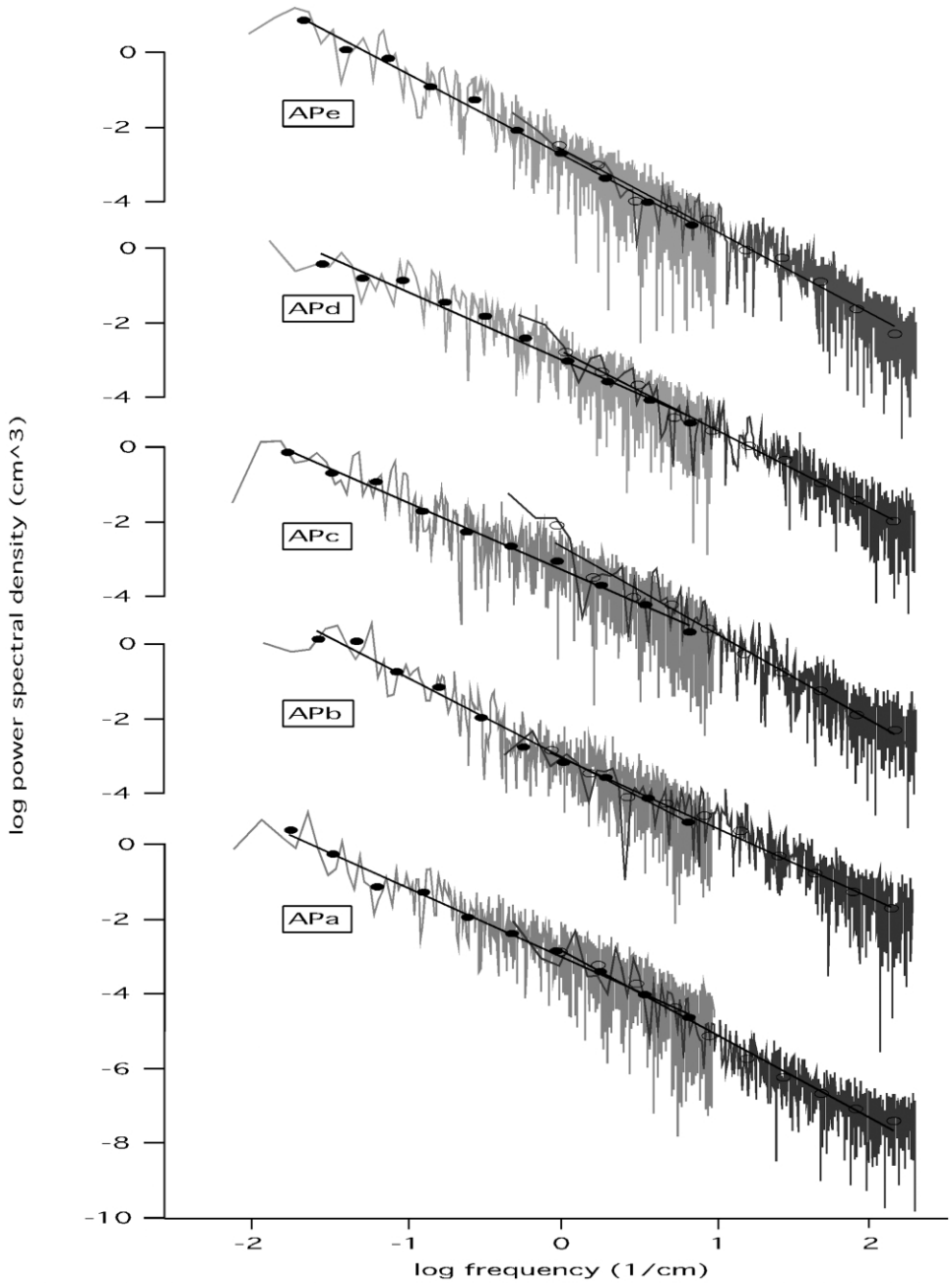

Fig. 6. Power spectra of Calcare Massiccio stylolites. The power spectra of the micro- (dark gray) and macro- (light gray) traces overlap in the 1–4.35 cm waveband. Open (closed) circles are averages of the binned spectra of micro (macro) traces. The regression lines are best fits to these averages.

the noise of the spectra, trading off on the extent of the trace (e.g. Welch, 1967). The results of this procedure are presented in Fig. 8. No break in slope or spike is apparent in the range of the dominant grain size (300–500 μm). We further note that the absence of any special features at the dominant grain size waveband for stylolites of the Tamar Formation (300–1000 μm) and the Skene Formation (50–200 μm) (Fig. 7).

Two micro-traces digitized at angles of +45° and −45° to the slab face of stylolite CMb were examined to determine the consistency of fractal properties throughout the plane of the stylolite. The spectra of these profiles are presented in Fig. 9. The fractal dimension of these profiles is similar to that of the slab-parallel profile, with an average of 1.58 (±0.04). Similar tests were performed on stylolites of the Tamar Formation (TMo2 and TMn2) yielding an average of 1.43 (±0.03) and of the Skene Formation (SKf1 and SKn1) yielding an average of 1.24 (±0.06).

Values of the fractal dimension and crossover length obtained by the SWV methods are listed in Table 3, and the curves for the LD method presented in Figs. 10 (Calcare Massiccio) and 11 (Tamar and Skene Formations). The fractal dimension obtained by the STD method was usually higher than that obtained by either LD or BD, though in

Table 2
The negative of the slope of the spectra (β), the fractal dimension (D_S) and the power at frequency 1/cm of stylolite profiles

Trace	β (± error)	D (± error)	pwr (mm)
Micro-CMa	2.25 (0.10)	1.37 (0.05)	17
Micro-CMb	1.87 (0.08)	1.57 (0.04)	11
Micro-CMc	2.34 (0.14)	1.33 (0.07)	24
Micro-CMd	2.11 (0.07)	1.44 (0.04)	22
Micro-CMe	2.21 (0.11)	1.4 (0.06)	26
Average micro-CM	2.16	1.42	20
sd micro-CM	0.18	0.09	6
Micro-CMbob1	1.92 (0.12)	1.54 (0.06)	9
Micro-CMbob2	1.75 (0.12)	1.62 (0.06)	5
Macro-CMa	1.86 (0.05)	1.57 (0.03)	11
Macro-CMb	2.13 (0.06)	1.44 (0.03)	12
Macro-CMc	1.82 (0.05)	1.59 (0.03)	6
Macro-CMd	1.84 (0.07)	1.58 (0.04)	13
Macro-CMe	2.18 (0.05)	1.41 (0.03)	18
Average macro-CM	1.96	1.52	12
sd macro-CM	0.18	0.09	4
TMn2	2.10 (0.13)	1.45 (0.07)	9
TMo2	2.20 (0.09)	1.4 (0.05)	8
Average TM	2.15	1.43	8
sd TM	0.07	0.04	1
SKf1l	2.42 (0.07)	1.29 (0.04)	4
SKf1u	2.39 (0.08)	1.31 (0.04)	4
SKn1	2.64 (0.13)	1.18 (0.07)	2
Average SK	2.48	1.26	4
sd SK	0.14	0.07	1

All values were obtained from spaced, detrended and tapered traces. β, D and pwr are slope, fractal dimension and power at frequency 1/cm from best fit to 10 equally spaced averages. All fits were trimmed from above and below to exclude highest and lowest frequencies. sd is standard deviation.

most cases not significantly so. The only exception to this rule was micro-trace CMa ($D_{STD} - D_{BD} = 0.18$) that has a very low fractal dimension (~1.1) where the STD method does not perform well (Cannon et al., 1997, their Fig. 6). In all other cases, the shapes of the curves of all three SWV methods as well as their values are similar. Breaks in slopes are apparent in the curves of macro-traces CMc, CMd and CMe, at a window size of ~10 cm, whereas gradual changes in slope are apparent in the curves of micro-traces CMb and CMe. Similar gradual changes in slope are seen in the curves of stylolites of the Tamar Formation (TMo2 and TMn2 in Fig. 11).

Self-similar analysis of stylolite contours by the ruler method is presented in Fig. 12. The fractal dimension of the stylolite contours in the Calcare Massiccio slab (CMdp2 and CMcp1) is 1.24, and that of stylolites in the Skene Formation (SKp2) and the 'Mystique Dark' tile (MDa1) is 1.12. The error bars in these curves indicate the range of 10 measurements with the same ruler size but with different starting points along the trace (see Middleton, 1999).

The Calcare Massiccio slab is ~99.5% carbonate, with trace amounts of chert, iron oxide aggregates and clays. The variation in residue content is presented in Table 4. Note that this variation is determined by the <75 μm fraction, because the complete residue contains relatively big fragments of chert and iron oxide aggregates that are randomly distributed and thus bias the measurement. The insoluble content in the stylolites (samples 2, 5, 8, 11 and 14 in Fig. 1 and Table 4) is larger than in the surrounding rock (samples 1 and 3, 4 and 6, 7 and 9, 10 and 12, and 13 and 15 in Fig. 1 and Table 4) by a factor of 2–7. These are underestimates because the stylolite cannot be completely separated from the ambient rock. For this reason it is impossible to accurately estimate the extent of dissolution along the stylolite by comparing the clay content in the stylolite and in the surrounding rock. However, it is obvious that the non-carbonate fraction is greater in the rock surrounding stylolites CMa and CMe than in that surrounding stylolites CMc and CMd.

Results of XRD analysis of the clay fraction are presented in Fig. 1 and Table 4. Kaolinite and illite are the predominant clay minerals throughout the rock (34–75% and 23–63%, respectively), whereas Fe-chlorite is far less abundant (<1%). The clay composition is consistent throughout the rock, though a slight increase in the kaolinite–illite ratio is observed from bottom to top of the slab. Furthermore, clay composition in any stylolite and the ambient rock on both its sides is identical. This indicates that the stylolites studied here were not unique sites of clay authigenesis. In addition, the apparent geometrical dissimilarities (i.e. those not resolved by our analysis) between these stylolites are probably not caused by clay composition.

5. Discussion

The fractal geometry of natural surfaces has been studied extensively in the past 20 years. Most of these surfaces are persistent fractional Brownian surfaces (Feder, 1988; Korvin, 1992), with fractal dimensions ranging between 1 and 1.5. The present study indicates that stylolites in the Calcare Massiccio are fractal over 4.5 orders of magnitude (10^{-5}–1 m), with average fractal dimension values of 1.47 (±0.1) determined by spectral analysis and 1.47 (±0.15) by the more reliable SWV methods. These values are relatively high, and reflect the obvious jaggedness of these stylolites. In addition, some stylolites from the Tamar and Skene Formation were shown to be fractal over three orders of magnitude (10^{-5}–10^{-2} m), with an average fractal dimension of 1.43 (1.43) and 1.24 (1.22) obtained by spectral analysis (SWV).

The fractal dimension of the Calcare Massiccio stylolites obtained by spectral analysis ranges from 1.33 to 1.57 (micro-traces) and 1.41 to 1.59 (macro-traces). The variations in fractal dimension reflect the apparent dissimilarity between some of the stylolites. For example, micro-trace CMa appears to be much smoother than micro-trace CMb, a fact registered in a lower fractal dimension for the

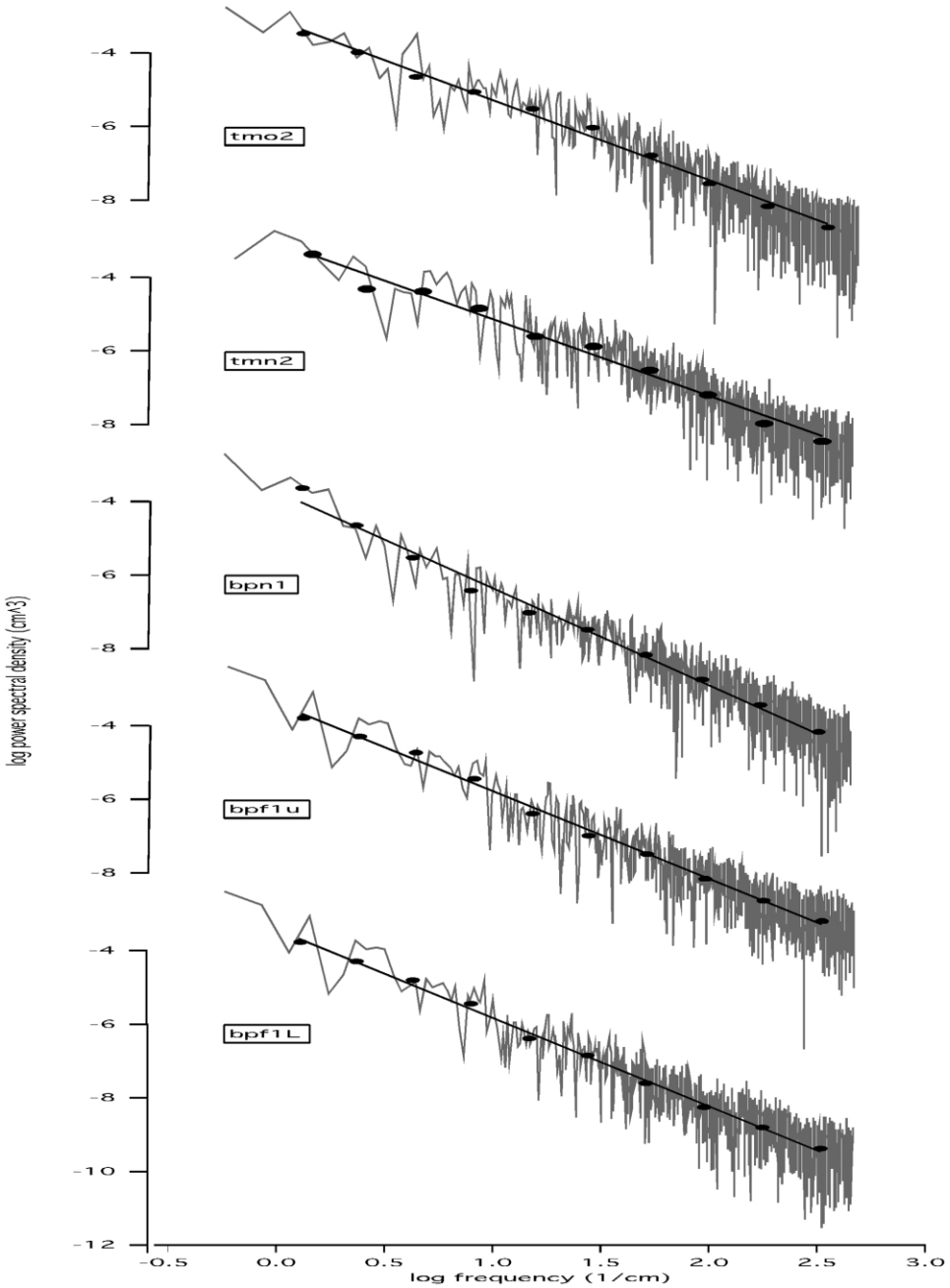

Fig. 7. Power spectra of stylolites from the Tamar (TM) and the Skene (SK) Formations. Closed circles are averages of the binned spectra of the traces. The regression lines are best fits to these averages.

first. However, this extreme case is on the limit of the resolution of the method ($\sim \pm 0.1$), so that statistically speaking the spectra of all other traces are indistinguishable. To increase the resolution of spectral analysis while maintaining its spatial extent one needs to stack the spectra of several long ($>2^{12}$ data points) profiles of the same stylolite (e.g. Brown and Scholz, 1985), which is technically unfeasible here.

The fractal dimension values of the Calcare Massiccio stylolites obtained by the linear regression SWV method (LD) range from 1.10 to 1.61, and are strongly correlated with those obtained by spectral analysis. (This correlation is better for the macro-traces, probably because they are three times longer than the micro-traces.) The average fractal dimension excluding micro-trace CMa (which has a fractal dimension of 1.1) is 1.51, and the standard deviation (0.08) lies well within the resolution of this method (Cannon et al., 1997). Therefore, the combined results of spectral and SWV analysis suggest that all stylolites in the Calcare Massiccio slab, excluding micro-trace CMa, have the same fractal dimension. A possible explanation for the low fractal dimension of micro-trace CMa is the high clay content of

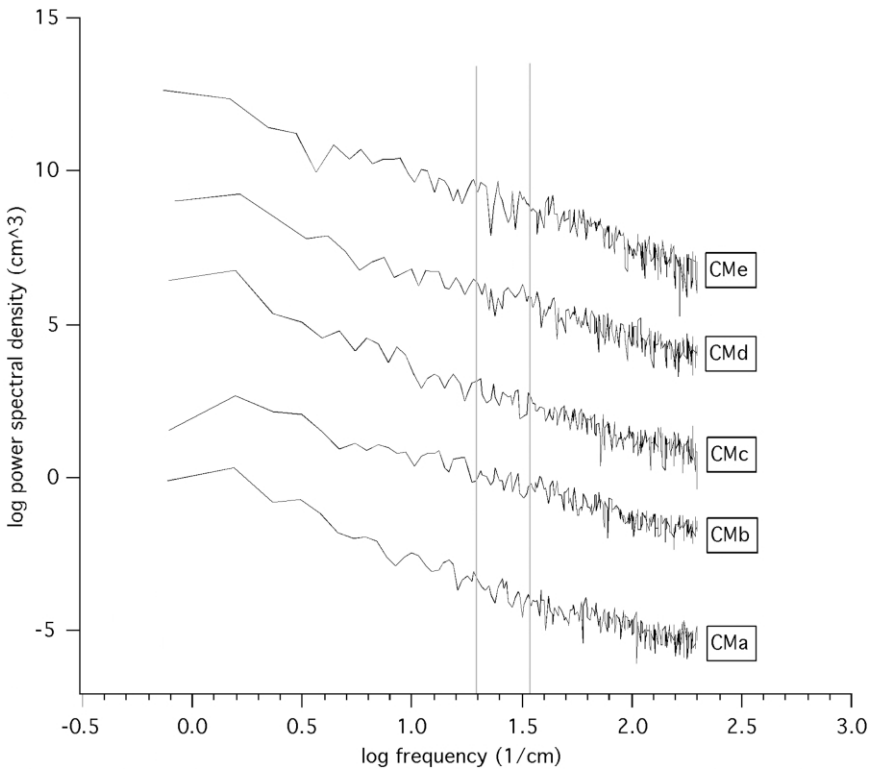

Fig. 8. Stacked power spectra of three ~500 points segments of each of the micro-traces of the Calcare Massiccio slab. The two vertical gray lines indicate 300 (right) and 500 (left) microns, which correspond to the dominant grain sizes in the slab (see Fig. 1).

Table 3
Fractal dimension (D) and crossover length (CO) of stylolite profiles determined by the standard windowed variability methods

Trace	DBD	COBD (cm)	DLD	COLD (cm)	DSTD	COSTD (cm)
Micro-CMa	1.09	0.91	1.1 (0.009)	0.90	1.27	0.72
Micro-CMb	1.56	0.51	1.57 (0.008)	0.51	1.63	0.45
Micro-CMc	1.34	0.67	1.33 (0.004)	0.68	1.39	0.60
Micro-CMd	1.49	0.55	1.51 (0.004)	0.54	1.51	0.51
Micro-CMe	1.52	0.52	1.51 (0.006)	0.54	1.55	0.48
Average micro-CM	1.40	0.63	1.41	0.63	1.47	0.55
sd micro-CM	0.19	0.17	0.19	0.16	0.14	0.11
Macro-CMa	1.58	0.46	1.57 (0.01)	0.48	1.61	0.41
Macro-CMb	1.45	0.58	1.45 (0.01)	0.59	1.54	0.47
Macro-CMc	1.61	0.46	1.60 (0.02)	0.47	1.67	0.38
Macro-CMd	1.58	0.44	1.57 (0.02)	0.45	1.63	0.37
Macro-CMe	1.46	0.55	1.44 (0.02)	0.57	1.55	0.43
Average macro-CM	1.53	0.50	1.53	0.51	1.60	0.41
sd macro-CM	0.07	0.06	0.07	0.06	0.05	0.04
TMn2	1.46	0.59	1.46 (0.01)	0.60	1.56	0.51
TMo2	1.40	0.65	1.40 (0.009)	0.66	1.50	0.56
average TM	1.43	0.62	1.43	0.63	1.53	0.54
sd TM	0.04	0.04	0.04	0.04	0.05	0.04
SKf1l	1.22	0.81	1.22 (0.005)	0.81	1.28	0.74
SKf1u	1.21	0.82	1.21 (0.006)	0.82	1.29	0.74
SKn1	1.23	0.82	1.25 (0.004)	0.81	1.25	0.79
Average SK	1.22	0.81	1.23	0.81	1.27	0.76
sd SK	0.01	0.01	0.02	0.00	0.02	0.03

BD—bridge detrending. LD—linear regression detrending. STD—no detrending. $D = 2 - H$, where D (fractal dimension) and H (Hurst exponent), is the slope of the regression line. CO (crossover length), is defined as the window length (w) where $f(w) = w$; f = BD, LD, STD. sd—standard deviation.

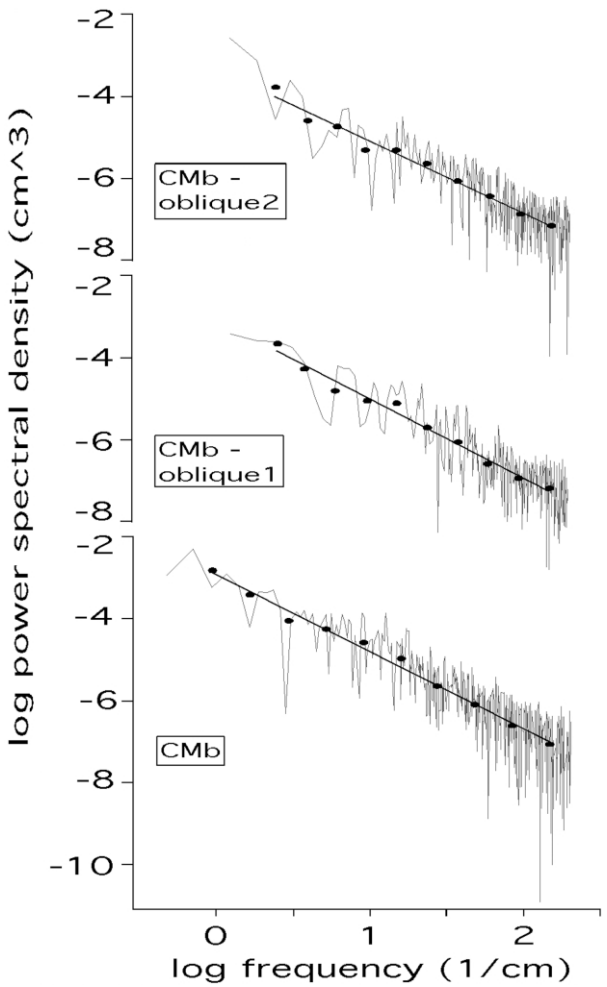

Fig. 9. Power spectra of micro-traces of stylolite CMb, parallel to the slab face (bottom) and at angles of +45° (center) and −45° (top) to the slab face.

the rock surrounding it (Table 4). Note that this does not affect the longer wavelengths as seen in the corresponding macro-trace.

The differences in fractal dimension in both spectral (Δ_{SA}) and SWV (Δ_{SWV}) analyses between micro-traces and their corresponding macro-traces is beneath the resolution, excluding stylolites CMa ($\Delta_{SA} = 0.20$ and $\Delta_{SWV} = 0.47$) and CMc ($\Delta_{SA} = 0.26$ and $\Delta_{SWV} = 0.27$). A possible cause for the low fractal dimension of micro-trace CMa was discussed earlier; a possible explanation for the uniqueness of stylolite CMc is that it bounds the greatest fabric contrast in the rock (Fig. 1). These examples may indicate a weak link between fractal dimension at short wavelengths and rock fabric and composition.

Grain size in the Calcare Massiccio slab ranges from <50 μm to over 1 cm, peaking at 300 μm for units 1 and 2, and 500 μm for units 3 and 4 (Fig. 1). These wavelengths do not register in the power spectra (Figs. 6 and 8), as expected considering similar studies on cracks and joints (e.g. Brown and Scholz, 1985). A similar absence of special features in the spectra at the grain waveband is observed for the traces of the Skene and Tamar Formations (Fig. 7). This indicates that grain size is not as important in controlling stylolite geometry as implied by some previous studies (e.g. Bathurst, 1991). We note that the grain size signal may be obliterated by the fact that grain size distribution in the rock is not uniform. However, if this result is significant, it indicates that the processes generating the serrated morphology are similar below and above the grain size.

Changes in slope in either spectra or SWV curves indicate transitions from one power law regime to another, reflecting a possible change in the underlying process (e.g. Pelletier and Turcotte, 1999), and are thus extremely important in fractal analysis. In this study breaks in slopes are seen in SWV curves of macro-traces CMc, CMd and CMe at a window size of ∼10 cm, and in the spectra of

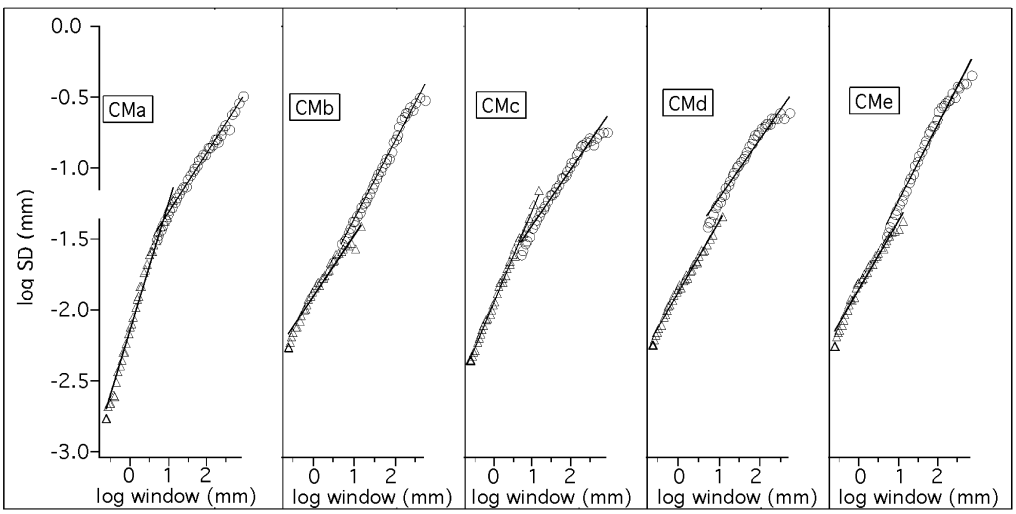

Fig. 10. Standard windowed variability analysis (linear regression detrending mode) of stylolites of the Calcare Massiccio Slab. Triangles are micro-traces and circles are macro-traces.

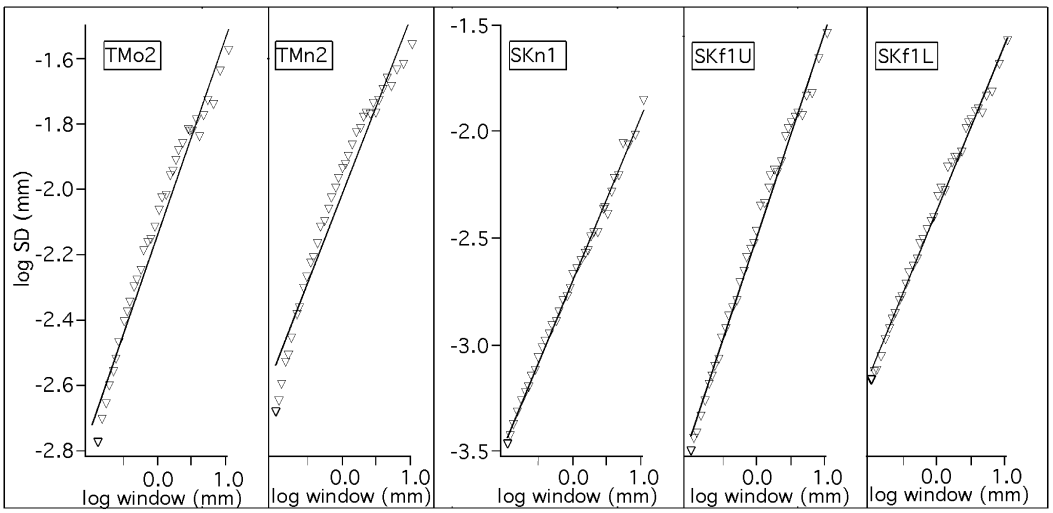

Fig. 11. Standard windowed variability analysis (linear regression detrending mode) of stylolites of the Skene and Tamar Formations.

macro-trace CMd and micro-traces CMa, CMb and CMc at wavebands of 10 cm and 1–3 mm, respectively. At this stage the significance of this result is not clear, especially since in most cases the break in slope of a given trace does not register in both analysis methods. One possible research path lies in a model presented by Gal et al. (1998), which assumes that the serrated geometry of stylolites is caused by gradients in strain and surface energies. Their model predicts the existence of a critical wavelength above which the stylolite grows and below which it flattens out. The critical wavelength λ_0 is given by:

$$\lambda_0 = \frac{\pi E \gamma}{(1-\nu^2)}\left[(P_1 - P_v)\left(P_1 - \frac{\nu}{1-\nu}P_v\right)\right]^{-1} \quad (3)$$

where E is the Young modulus, γ the surface energy, ν the Poisson ratio and P_1 and P_v the lateral and vertical stresses, respectively. Using appropriate values for a limestone-water system ($E = 6 \times 10^{10}$ Pa, $\gamma = 10$ J/m^2, $\nu = 0.3$), assuming lithostatic and hydrostatic stresses, and an average density of 2570 kg/m^3, for $\lambda_0 = 10$ cm we obtain a depth of ~ 1 km. Note that Gal's critical wavelength depends solely on the bulk mechanical properties of the rock, and is independent of grain size. The physical significance of the critical wavelength was not discussed by Gal et al. (1998), and is yet to be investigated.

Preliminary results indicate that the fractal properties of stylolite profiles are not orientation-dependent, i.e. fractal dimension and power are the same in all directions on the stylolite surface. This is a significant result, since in most observational and theoretical studies stylolites are treated as two-dimensional features. The present study suggests that any two-dimensional profile of a stylolite is statistically representative of the stylolite surface. Because amplitudes decrease gradually towards the stylolite tip, and increase gradually towards coexisting cracks (Smith, 2000), our statement is restricted to the undisturbed center part of the stylolite. A more thorough 3D study is clearly needed at this point.

Finally, the stylolites were shown to maintain fractal geometry in cross-sections parallel to their plane. These traces, termed contours here, are shown to be fractal with a fractal dimension ($D_{contour}$) lower than that of the corresponding profiles ($D_{profile}$), though determined by a different, less robust method. We note that Huang and

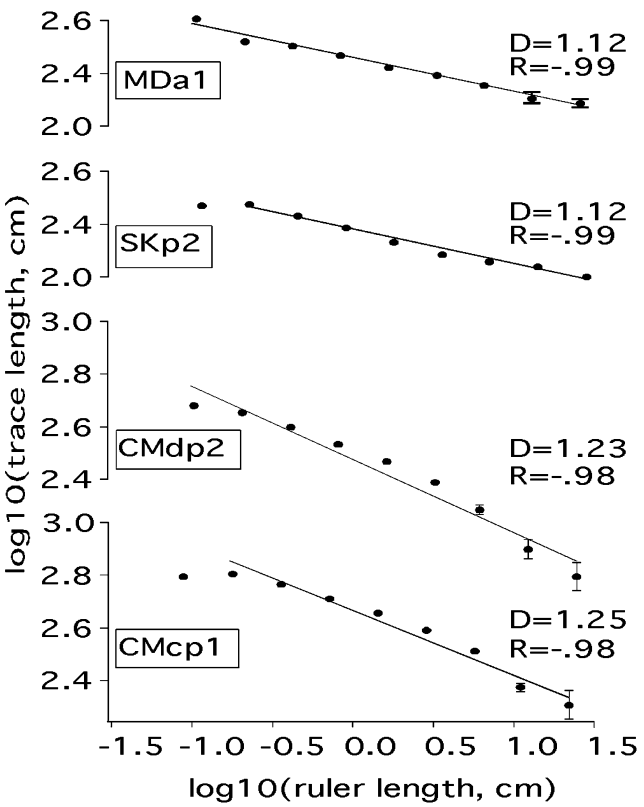

Fig. 12. Analysis of self-similar contours of stylolites from the Calcare Massiccio slab (CMcp1 and CMdp2), the Skene Formation (SKp2) and the Mystique Dark tile (MDa1), by the ruler method (see Fig. 4). The error bars indicate the range of 10 measurements with the same ruler size but with different starting points along the trace.

Table 4
Insoluble residue content and clay composition of the studied rock slab. Insoluble residue content was determined on the <75 μm fraction. Residues are 2–7 times larger in the stylolites than in their respective ambient rock. Clay composition was determined on the <2 μm fraction by XRD. Sample location is shown in Fig. 1

Sample no.	Location[a]	Insoluble residue (%)[b]	Chlorite (%)[c]	Illite (%)	Kaolinite (%)	C + I + K	K/I
1	Below CMa	0.18	0.05	41.66	56.31	98.01	1.35
2	CMa	1.37	0.37	42.94	54.75	98.07	1.28
3	Above CMa	0.17	0.22	43.51	54.81	98.54	1.26
4	Below CMb	0.16	0.00	62.80	33.95	96.75	0.54
5	CMb	0.30	0.20	52.56	44.66	97.42	0.85
6	Above CMb	0.10					
7	Below CMc	0.12	0.13	47.29	51.26	98.67	1.08
8	CMc	0.33	0.00	43.34	54.59	97.93	1.26
9	Above CMc	0.09	0.34	36.98	59.94	97.27	1.62
10	Below CMd	0.08	0.00	22.46	74.68	97.15	3.32
11	CMd	0.17	0.07	43.43	54.30	97.80	1.25
12	Above CMd	0.09	0.28	29.24	67.99	97.50	2.33
13	Below CMe	0.13	0.84	29.91	61.16	91.91	2.04
14	CMe	0.35	0.06	27.41	68.04	95.51	2.48
15	Above CMe	0.17	0.18	30.31	66.08	96.56	2.18

[a] See Fig. 1.
[b] Insoluble residue was determined on the <75 micron fraction.
[c] Clay composition was determined on the <2 micron fraction.

Turcotte (1989) actually showed that the fractal dimension of a 2D surface is not directly related to that of its profile by adding one, as previously suggested by others (e.g. Voss, 1988). Our results may imply that any cross-section through a stylolite, no matter its inclination with respect to the plane of the stylolite, will be fractal, with a fractal dimension ranging from $D_{contour}$ to $D_{profile}$. Furthermore, these contours may provide some insight into the lateral growth of stylolites and warrant further research.

Drummond and Sexton (1998) obtained a D_S of 1.35 for a 12 cm segment of a stylolite in Salem Limestone, at wavelengths of 0.37–38 mm. We note the similarity in values, but recognize that a comparison between the present study and others demands a more detailed investigation of both the rock and the analytical procedure.

Recently, Hassan et al. (2002) studied 22 stylolite samples (up to 12 cm long) from the carbonate Khuff Formation (Permian, Saudi Arabia), to determine the relationship between their morphology and their fractal properties. They obtained by the box counting method (see Feder, 1988) fractal dimension values ranging from 0.95 to 1.35. Combined with Hurst coefficient values obtained by R/S analysis, they present a positive correlation between the fractal dimension and the stylolite complexity, as defined qualitatively by Park and Schot (1968), i.e. the more complex the stylolite the higher its fractal dimension. The Calcare Massiccio stylolites studied here are 'seismogram-like', and are classified as 'complex', thus their high fractal dimension agrees with the Hassan et al. (2002) assertion.

Railsback (1993) studied the relationship between stylolite geometry and rock fabric in Paleozoic carbonates. He concluded that vertical offsets (his O parameter, analogous to amplitude) and 'frequency' (his F parameter, defined as number of vertical offsets per length) is roughly positively correlated with grain to mud ratio, thus implying a link between stylolite geometry and rock fabric. We first note that when applying Railsback's geometrical scheme to seismogram-type stylolites one should be aware of their fractal nature—the number of features counted strongly depends on the scale of observation. Second, here we focused on another parameter of rock fabric, the grain size, and showed that it does not register in the fractal analyses. However, we note that despite the distinct difference in mud-grain-cement ratio in the Calcare Massiccio slab between the lower and upper parts of the slab (Fig. 1) the fractal dimension of the stylolites in the slab is similar.

6. Conclusions

The present study and others establish that stylolites are fractal surfaces. Our study, however, is unique in the extent of the waveband analyzed, the consideration of traces at various orientations with respect to the stylolite plane and the robustness of the analysis. What does the fact that stylolites are fractal tell us about the processes that generated them? Fractal geometry exhibits long-range correlation, implying that dissolution and precipitation at one point along the stylolite impacts dissolution and precipitation at other points (e.g. Aharonov and Rothman, 1996). Clearly any model of stylolite formation should exhibit this feature. Renard et al. (1999) suggested that grain scale pressure solution processes are power-law, and modeled the grain contact evolution through a percolation law. The latter is a classic example of phenomena termed self-organization criticality (Turcotte, 1992), that are known

to produce fractal distributions and structures (e.g. Bak and Tang, 1989). In the present study we showed that stylolites are fractal and that the grain size does not affect their fractal geometry. We thus suggest that a power law process, similar to those generating island-channel structures at grain contacts, may be responsible for the formation and evolution of stylolites.

Fletcher and Pollard (1981) proposed that stylolites are 'anti-cracks', dissolution surfaces that grow laterally due to stress concentration at their tips. Their model did not address the serrated geometry of stylolites, but merely the fact that the amplitudes are largest in the middle and taper off towards the tips. By association with cracks, which have been shown to be fractal (e.g. Brown and Scholz, 1985), anti-cracks were assumed to be fractal too. And indeed, Riggs and Green (2001) have recently shown that synthetic high temperature and pressure anti-cracks are fractal. Our results agree with this feature of the anti-crack model. In addition, the anti-crack model implies a scaling relationship between length and displacement (e.g. Mardon, 1988; Scholz et al., 1993). Though intrinsically more complicated to measure than for cracks and faults, length and displacement values for stylolites, combined with fractal dimension estimates reported here, should provide a powerful tool for constraining models of stylolite formation and propagation. This is especially important considering the scaling relationship between jaggedness and formation time for growth models of various fractal surfaces (e.g. ballistic deposition; Barabasi and Stanley, 1995).

Finally, what is the significance of the overall similarity of fractal dimension of all the Calcare Massiccio stylolites studied here? Assuming that all five stylolites evolved through mass transfer creep and at approximately the same time, and taking into account the variations in fabric and composition in the rock surrounding each stylolite, we suggest that local properties are not dominant in determining the fractal geometry of these stylolites, especially at long wavelengths. Obviously this hypothesis should be further tested on a broader range of lithologies and for different types of stylolites. For example, this statement may not hold for rocks consisting of relatively large grains such as brachipod shells embedded in a finer, more soluble matrix. In such a case, stylolites are often observed to have a rectangular morphology with the brachiopod shells capping the columns, and thus the fabric essentially controls its geometry.

Acknowledgements

We wish to thank Ted Koczynski for technical support and Pierre Biscaye and Adele Hanley for guidance in clay analysis. Charlie Mandeville kindly provided access to the optical microscope at the American Museum of Natural History. The Calcare Massiccio slab was bought at Dente Trading Co. in Cedar Grove, New Jersey, and identified by Giorgio Parisi and Lucio D'Alberto. We thank Alberto Malinverno and Einat Aharonov for discussions on fractals and stylolites, and Spahr Webb for discussions on time series analysis. Reviews by Bruce Railsback and Tom Blankinsop improved the text significantly. This research was sponsored by U.S. National Science Foundation award EAR00-00947. This is Lamont-Doherty Earth Observatory contribution 6375.

References

Aharonov, E., Rothman, D.H., 1996. Growth of correlated pore-scale structures in sedimentary rocks: a dynamical model. Journal of Geophysical Research 101, 2973–2987.

Alvarez, W., Engelder, T., Geiser, P.A., 1978. Classification of solution cleavage in pelagic limestones. Geology 6, 263–266.

Bak, P., Tang, C., 1989. Earthquakes as a self-organized critical phenomena. Journal of Geophysical Research 94, 15,635–15,637.

Barabasi, A.L., Stanley, H.E., 1995. Fractal Concepts in Surface Growth, Cambridge University Press, New York.

Barrett, P.J., 1964. Residual seams and cementation in Oligocene shell calcarenites, Te Kuiti group. Journal of Sedimentary Petrology 34, 524–531.

Bassingthwaighte, J.B., Raymond, G.M., 1994. Evaluating rescaled range analysis for time series. Annals of Biomedical Engineers 22, 432–444.

Bassingthwaighte, J.B., Raymond, G.M., 1995. Evaluation of the dispersional analysis method for fractal time series. Annals of Biomedical Engineers 23, 491–505.

Bathurst, R.G.C., 1991. Pressure solution and limestone bedding: the influence of stratified cementation. In: Einsele, G., Ricken, W., Seilacher, A. (Eds.), Cycles and Events in Stratigraphy, Springer-Verlag, Berlin, pp. 3–15.

Bathurst, R.G.C., 1995. Burial diagenesis of limestones under simple overburden: stylolites, cementation and feedback. Bulletin De La Societe Geologique De France 166, 181–192.

Biscaye, P.E., 1965. Mineralogy and sedimentation of recent deep-sea clay in the Atlantic Ocean and adjacent seas and oceans. Geological Society of America Bulletin 76, 803–832.

Bos, B.C., Peach, C.J., Spiers, C.J., 2000. Slip behavior of simulated gouge-bearing faults under conditions favoring pressure solution. Journal of Geophysical Research 105, 16699–16717.

Brown, S., Scholz, C.H., 1985. Broad bandwidth study of the topography of natural rock surfaces. Journal of Geophysical Research 90, 12,575–12,582.

Cannon, M.J., Percival, D.B., Caccia, D.C., Raymond, G.M., Bassingthwaighte, J.B., 1997. Evaluating scaled windowed variance methods for estimating the Hurst coefficient of time series. Physica A 241, 606–626.

Den Brok, S.W.J., 1998. Effects of microcracking on pressure-solution strain rate: the Gratz grain-boundary model. Geology 26, 915–918.

Dewers, T., Ortoleva, P., 1990. A coupled reaction/transport/mechanical model for intergranular pressure solution, stylolites, and differential compaction and cementation in clean sandstones. Geochimica et Cosmochimica Acta 54, 1609–1625.

Dolan, J.F., Sieh, K., Rockwell, T.K., Yeats, R.S., Shaw, J., Suppe, J., Huftile, G.J., Gath, E.M., 1995. Prospect for larger or more frequent earthquakes in the Los Angeles metropolitan region. Science 267, 199–205.

Drummond, C.N., Sexton, D.N., 1998. Fractal structure of stylolites. Journal of Sedimentary Research 68, 8–10.

Duebendorfer, E.M., Vermilye, J., Geiser, P.A., Davis, T.L., 1998. Evidence for aseismic deformation in the western Transverse Ranges,

southern California: implications for seismic risk assessment. Geology 26, 271–274.
Eke, A., Herman, P., Kocsis, L., Kozak, L.R., 2002. Fractal characterization of complexity in temporal physiological signals. Physiological Measurements 23, R1–R38.
Feder, J., 1988. Fractals, Plenum Press, New York.
Fletcher, R.C., Pollard, D.D., 1981. Anticrack model for pressure solution surfaces. Geology 9, 419–424.
Gal, D., Nur, A., Aharonov, E., 1998. Stability analysis of a pressure-solution surface. Geophysical Research Letters 25, 1237–1240.
Guzzetta, G., 1984. Kinematics of stylolite formation and physics of the pressure-solution process. Tectonophysics 101, 383–394.
Hassan, M.H., Korvin, G., Abdulraheem, A., 2002. Fractal and genetic aspects of Khuff reservoir stylolites, Eastern Saudi Arabia. Arabian Journal for Sciences and Engineering 27, 29–56.
Heald, M.T., 1955. Stylolites in sandstones. The Journal of Geology 63, 101–114.
Hickman, S.H., Evans, B., 1995. Kinetics of pressure solution at halite–silica interfaces and intergranular clay films. Journal of Geophysical Research 100, 13,113–13,132.
Huang, J., Turcotte, D.L., 1989. Fractal mapping of digitized images: application to the topography of Arizona and comparisons with synthetic images. Journal of Geophysical Research 94, 7491–7495.
Hurst, H.E., 1951. Long-term storage capacity of reservoirs. Transactions of the American Society of Civil Engineers 116, 770–808.
Hurst, H.E., Black, R.P., Simaika, Y.M., 1965. Long-term Storage: An Experimental Study, Constable, London.
Kanagawa, K., Cox, S.F., Zhang, S., 2000. Effects of dissolution–precipitation processes on the strength and mechanical behavior of quartz gouge at high-temperature hydrothermal conditions. Journal of Geophysical Research 105, 11115–11126.
Korvin, G., 1992. Fractal Models in the Earth Sciences, Elsevier Science Publishers, Amsterdam.
Langer, V.W., Novakowski, K.S., Woodbury, A.D., 1999. Sorption of trichloroethene onto stylolites. Journal of Contaminant Hydrology 40, 1–23.
Lind, I., Schioler, P., 1994. Dinoflagellate cyst concentration as an independent reference for monitoring mineral mobilization in stylolites. Sedimentary Geology 92, 53–65.
Malamud, B.D., Turcotte, D., 1999. Self affine time series: I. Generation and analyses. Advances in Geophysics 40, 1–90.
Malinverno, A., 1990. A simple method to estimate the fractal dimension of a self-affine series. Geophysical Research Letters 17, 1953–1956.
Malinverno, A., 1991. Fractals and their use in the Earth Sciences. Unpublished.
Mardon, D., 1988. Localization of pressure solution and the formation of discrete solution seams. Ph.D. thesis, Texas A&M University.
Middleton, G.V., 1999. Data Analysis in the Earth Sciences using MATLAB, Prentice Hall, New Jersey.
North, R.G., 1974. Seismic slip rates in the Mediterranean and Middle East. Nature 252, 560–563.
Ortoleva, P., Al-Shaieb, Z., Puckette, J., 1995. Genesis and dynamics of basin compartments and seals. American Journal of Science 295, 345–427.
Park, W.C., Schot, E.H., 1968. Stylolites: their nature and origin. Journal of Sedimentary Petrology 38, 175–191.
Paterson, M.S., 1973. Nonhydrostatic thermodynamics and its geologic applications. Reviews of Geophysics and Space Physics 11, 355–389.
Pelletier, J.D., Turcotte, D.L., 1999. Self affine time series: II. Applications and models. Advances in Geophysics 40, 91–174.
Press, W.H., Teukolsky, S.A., Vetterling, W.T., Flannery, B.P., 1994. Numerical Recipes in C: The Art of Scientific Computing, Cambridge University Press, Cambridge.
Railsback, L.B., 1993. Lithologic controls on morphology of pressure–dissolution surfaces (stylolites and dissolution seams) in Paleozoic carbonate rocks from the Mideastern US. Journal of Sedimentary Petrology 63, 513–522.
Renard, F., Park, A., Ortoleva, P., Gratier, J.P., 1999. An integrated model for transitional pressure solution in sandstones. Tectonophysics 312, 97–115.
Riggs, E.M., Green, H.W., 2001. Shear localization in transformation-induced faulting: first order similarities to brittle shear failure. Tectonophysics 340, 95–107.
Rutter, E.H., 1983. Pressure solution in nature, theory and experiment. Journal of the Geological Society of London 140, 725–740.
Scholz, C.H., 1995. Fractal transitions on geological surfaces. In: Barton, C.C., La Pointe, P.R. (Eds.), Fractals in the Earth Sciences, Plenum Press, New York.
Scholz, C.H., Dawers, N.H., Yu, J.Z., Anders, M.H., 1993. Fault growth and fault scaling laws: preliminary results. Journal of Geophysical Research 98, 21,951–21,961.
Sleep, N.H., Blanpied, M.L., 1992. Creep, compaction and the weak rheology of major faults. Nature 359, 687–692.
Smith, J.V., 2000. Three-dimensional morphology and connectivity of stylolites hyperactivated during veining. Journal of Structural Geology 22, 59–64.
Stockdale, P.B., 1922. Stylolites: their nature and origin. Indiana University Studies IX, 1–97.
Stockdale, P.B., 1926. The stratigraphic significance of solution in rocks. Journal of Geology 34, 399–414.
Tada, R., Siever, R., 1989. Pressure solution during diagenesis. Annual Reviews Earth and Planetary Sciences 17, 89–118.
Turcotte, D.L., 1992. Fractals and Chaos in Geology and Geophysics, Cambridge University Press, Cambridge.
Voss, R.F., 1988. Fractals in nature: from characterization to simulation. In: Peitjen, H.O., Saupe, D. (Eds.), The Science of Fractal Images, Springer Verlag, New York, pp. 21–70.
Wanless, H.R., 1979. Limestone response to stress: pressure solution and dolomitization. Journal of Sedimentary Petrology 49, 437–462.
Welch, P.D., 1967. The use of fast Fourier transform for the estimation of power spectra: a method based on time averaging over short modified periodograms. IEEE Transactions, Audio and Electroacoustics AU-15, 70–73.
Wilson, T.H., 2000. Some distinctions between self-similar and self-affine estimates of fractal dimension with case history. Mathematical Geology 32, 319–335.